34th AIAA Fluid Dynamics Conference and Exhibit, June 28–July 1 2004, Portland OR

Local Adaption and Dissipation Properties of a Weighted Essentially Non-Oscillatory Scheme

Ellen M. Taylor * and M. Pino Martín †
Princeton University, Princeton NJ 08544

V. Gregory Weirs ‡
University of Chicago, Chicago IL 60637

We perform several direct numerical simulations (DNS) of decaying isotropic turbulence with various initial turbulent mach numbers M_t using a modified[1] weighted essentially non-oscillatory (WENO) method. We then present a procedure for the identification of shock-containing and smooth regions where the WENO scheme should respectively engage its adaption mechanism and revert to its linear optimal stencil. Weirs[1] has previously proposed the centrality index CI and nonlinearity index NI as two quantitative measures of stencil adaption, and we analyze these values within the regions of interest in the DNS flow fields. Our preliminary results indicate that these indices are suitable for assessments of the local adaption and dissipation properties of the WENO method; however, further studies must be conducted over a wider range of compressible flow conditions.

I. Introduction

The relevant structures of turbulence span a large range of length scales, and thus the detailed simulation of turbulent flow fields requires numerical methods that avoid excessive damping of features nearly as small as the grid spacing. This in turn demands high order of accuracy and high bandwidth-resolving efficiency. Though many such methods are available, compressible flows introduce the possible presence of shocks and shocklets, which are small transient shocks. If a high-order numerical method is employed across a shock, spurious oscillations, often indistinguishable from turbulent fluctuations, will arise and continuously grow over time. These oscillations may cause the simulation to crash or return results that are unreliable. One answer to this problem is the class of methods known as weighted essentially non-oscillatory (WENO) schemes.

WENO schemes, which were first cast into finite-difference form by Jiang and Shu,[2] compute the numerical fluxes at a given point via a number of different candidate stencils and form the final flux approximation by summing weighted contributions from each stencil. Smoothness measurements cause stencils that span large flow field gradients to be assigned small relative weights so that a nearly-discontinuous shock would provide a weight of almost zero to any stencil containing it. In completely smooth regions, the relative values of the weights are designed to be optimal by some gauge such as maximum order of accuracy or maximum bandwidth. This weighting procedure causes the WENO schemes to be more robust than their predecessors, the essentially non-oscillatory (ENO) schemes, which used only the single smoothest stencil to the exclusion of the others.

The detailed simulation of turbulence is performed through direct numerical simulation (DNS) or large-eddy simulation (LES). While DNS fully resolves all turbulent length and time scales, LES relies on turbulence modeling for the smaller scales to allow the computational grid to be coarsened beyond the capabilities of DNS. Garnier et al.[3] demonstrated that in LES of decaying isotropic turbulence the global dissipation of a variety of shock-capturing methods, including the standard WENO scheme,[2] overpowered the inherent dissipation of the sub-grid scale turbulence model. Recently, however, Weirs[1] successfully mitigated sources

*Ph.D. Student, Mechanical and Aerospace Engineering
†Assistant Professor, Mechanical and Aerospace Engineering
‡Research Scientist, ASC Flash Center

of dissipation in Jiang and Shu's scheme[2] and thereby improved its performance. In theory, Weirs' symmetric optimal stencils eliminate nearly all dissipation that occurs when the adaption mechanism is disengaged.[1] Martín[4,5] and Xu and Martín[6] have shown that this modified WENO method provides accurate results for DNS of turbulence, but Martín[7] has also concluded that in LES the global numerical dissipation is still excessive due to insufficient distinction between shock-containing and smooth regions.

The purpose of this paper is to provide a foundation for investigations and improvements of WENO schemes in the context of LES. We first analyze the characteristics of the WENO method in DNS, for which it produces satisfactory results. Using the DNS data, we search for shock-containing and smooth flow regions and assess the local adaption properties of the modified WENO scheme. Our primary goal is to identify reliable quantitative measures of stencil adaption that will aid future studies of WENO properties in LES. In the remainder of the paper, we present the governing equations, the details of the numerical simulations, a procedure to identify shocklets and shock-free regions, and indices of WENO stencil adaption. Finally, we discuss our results.

II. Governing Equations

The equations governing the motion of a compressible fluid are the Navier-Stokes equations describing the conservation of mass, momemtum, and energy,

$$\frac{\partial \rho}{\partial t} + \frac{\partial}{\partial x_k}\left(\rho u_k\right) = 0 \tag{1}$$

$$\frac{\partial}{\partial t}\left(\rho u_i\right) + \frac{\partial}{\partial x_k}\left(\rho u_i u_k + p\delta_{ik} - \sigma_{ik}\right) = 0 \tag{2}$$

$$\frac{\partial}{\partial t}\left(\rho e\right) + \frac{\partial}{\partial x_k}\left[\left(\rho e + p\right) u_k - \sigma_{kl} u_l + q_k\right] = 0 \tag{3}$$

in which ρ is the density, u_i is the velocity in the i direction, and p is the pressure. The shear stress tensor σ_{ij} is assumed to obey a linear stress-strain relationship,

$$\sigma_{ij} = \mu\left[\left(\frac{\partial u_i}{\partial x_j} + \frac{\partial u_j}{\partial x_i}\right) - \frac{2}{3}\frac{\partial u_k}{\partial x_k}\delta_{ij}\right] \tag{4}$$

in which the viscosity μ depends only on the temperature T through a power law,

$$\mu = \mu_0\left(\frac{T}{T_0}\right)^n \tag{5}$$

Our working fluid is air, which we treat as a perfect gas with a gas constant R and a constant specific heat capacity (at constant volume) c_v. The total energy per unit mass e is given by

$$e = c_v T + \frac{1}{2}u_k u_k \tag{6}$$

The heat flux in the i direction q_i arises from conduction through Fourier's law,

$$q_i = -\kappa\frac{\partial T}{\partial x_i} \tag{7}$$

in which the thermal conductivity κ is directly related to μ as

$$\kappa = \left(\frac{5}{2}c_v - \frac{3}{2}R\right)\mu \tag{8}$$

III. Weirs' Modified WENO Scheme

We shall summarize the operation of the modified WENO method of Weirs[1] in the context of the scalar, one-dimensional advection equation,

$$\frac{\partial u}{\partial t} + \frac{\partial}{\partial x} f(u) = 0 \tag{9}$$

If the spatial domain is discretized such that $x_i = i\Delta$, in which Δ is the grid spacing, and $u_i = u(x_i)$, equation (9) may be cast into the semidiscretized form

$$\frac{du_i}{dt} = -\frac{1}{\Delta}\left(\hat{f}_{i+\frac{1}{2}} - \hat{f}_{i-\frac{1}{2}}\right) \tag{10}$$

in which $\hat{f}_{i+\frac{1}{2}}$ is a numerical approximation of $f\left(u(x_{i+\frac{1}{2}})\right)$. Once the right-hand side of equation (10) has been evaluated, numerical techniques for solving ordinary differential equations, such as Runge-Kutta methods, may be employed to advance the solution in time. In order to ensure stability, procedures that approximate $f(u)$ generally split it into $f^+(u)$, which has a strictly non-negative derivative, and $f^-(u)$, which has a strictly non-positive one.

WENO schemes compute $\hat{f}^+_{i+\frac{1}{2}}$ through interpolating polynomials on a number r of candidate stencils. In the modified WENO method, each stencil contains r grid points. The one fully upwinded stencil ranges from $(i-r+1)$ to i, the one fully downwinded stencil ranges from $(i+1)$ to $(i+r)$, and the other stencils fall in between these two extremes. This collection of stencils is symmetric about the point $(i+\frac{1}{2})$. If the flux approximation on stencil k is designated q_k and the weight assigned to that stencil is ω_k, the final numerical approximation becomes

$$\hat{f}^+_{i+\frac{1}{2}} = \sum_{k=0}^{r} \omega_k q_k \tag{11}$$

In completely smooth regions, every stencil is equally desirable, and the weights revert to the optimal weights C_k. Because the total number of data points available to the modified WENO algorithm is $2r$, its maximum order of accuracy is also $2r$. In practice, the weight of the fully downwinded stencil ω_r is artificially constrained to be no greater than the least of the others so that adverse stability effects are avoided.

IV. Numerical Simulations

Because our goal is to study the adaption mechanism of the WENO method in a context relevant to compressible turbulence, we have chosen to simulate decaying isotropic turbulence. Isotropic turbulence is a canonical flow field that realistically represents the small scales of many turbulent flows. The global strength of these turbulent fluctuations decays over time without external forcing, which we have not included.

The physical domain is a three-dimensional cube with periodic boundary conditions and an edge length such that the large-scale turbulence statistics are sufficiently uncorrelated between its center and edges. An evenly-spaced Cartesian grid discretizes this cube into N^3 points. The governing parameters for the generation of the initial field are an average density ρ and temperature T; the average turbulent Mach number $M_t = \frac{q}{a}$, in which a is the average speed of sound and q is the root-mean-squared velocity summed over all three directions; the Reynolds number based on the Taylor microscale $Re_\lambda = \frac{\rho u' \lambda}{\mu}$, in which u' is the root-mean-squared velocity and λ is the Taylor microscale; and the nondimensional wavenumber magnitude at which the energy spectrum peaks k_0.

For the first stage of the initialization of isotropic turbulence, the density and temperature throughout the domain are constrained to be uniform, and each velocity component at each grid point is assigned a random number in the range $[-0.5 : 0.5]$. The physical velocity field is then transformed into Fourier space where its compressible part is removed to form a solenoidal field. This field is normalized so that the turbulent kinetic energy spectrum conforms to the approximate relation

$$E(k) = A\ k^4 e^{-2(k/k_0)^2} \tag{12}$$

in which A is a constant of proportionality that depends on q and k_0. Blaisdell and Ristorcelli[8] have presented methods by which to add consistent dilatation and density and pressure fluctuations; however, these rely on

pertubation techniques that may be applied when M_t is small, which is not true of the conditions that we consider. Thus, our initial flow fields are solendoidal.

We evolve the initial field through DNS using a third-order Runge-Kutta time integration scheme. To compute the convective numerical fluxes we use a fourth-order, bandwidth-optimized WENO scheme,[1] and for the viscous fluxes, which are diffusive in nature, we use a fourth-order central standard (order-optimized) scheme. A field is deemed to have reached a proper state of isotropic turbulence when the skewness of the velocity derivatives becomes relatively steady at roughly -0.5.

We have chosen to perform simulations under the following conditions:

Table 1. Governing Parameters

	M_t	Re_λ	ρ	T	k_0
Run 0	0.3	35	1	300	4
Runs 1 & 2	0.6	35	1	300	4
Runs 3 & 4	0.7	35	1	300	4
Runs 5 & 6	0.8	35	1	300	4

In each case, the number of grid points required for grid-convergence is 128^3. Different runs with the same governing parameters use varying seeds to generate the random numbers for the initialization of the velocity field. We have included a validation run, Run 0, in order to compare the results of the WENO method to those of a well-established Padé scheme,[9,10] and Fig. 1 demonstrates the agreement between the two. Figure 2 shows the temporal evolution of the skewness of the velocity derivatives for the remaining runs. From this we judge that each of the simulations has reached a proper state of isotropic turbulence at a nondimensional time of 1.5. The reference time for the nondimensionalization is $\tau_t = \frac{\lambda}{u'}$.

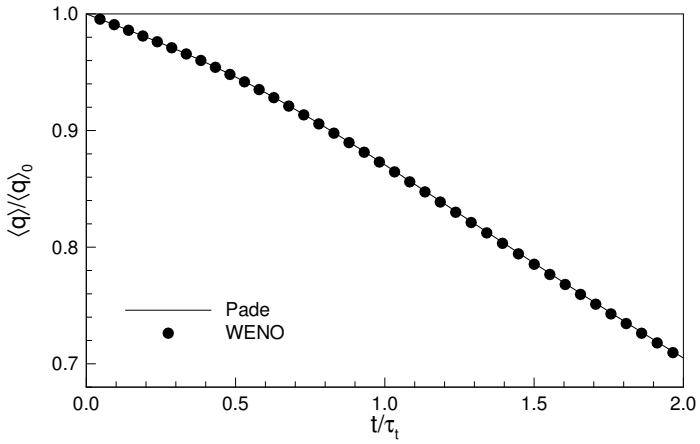

Figure 1. Temporal evolution of the root-mean-squared velocity q for Run 0.

The flow fields that we analyze throughout the remainder of this paper are those recorded after halting each simulation at $\frac{t}{\tau_t} = 1.5$. The temporal evolution of the average M_t up to this point is displayed in Fig. 3. The final M_t ranges from 0.45 for an initial $M_t = 0.6$ to 0.58 for an initial $M_t = 0.8$, and we realize that our simulations of isotropic turbulence may consequentially be limited in providing significantly diverse shock strengths.

V. Shocklets and Shock-Free Regions

Within the data that we have obtained we wish to locate shocklets, for which the WENO scheme was originally designed and where it should adapt, and compare them to smooth regions, where the WENO scheme should not adapt.

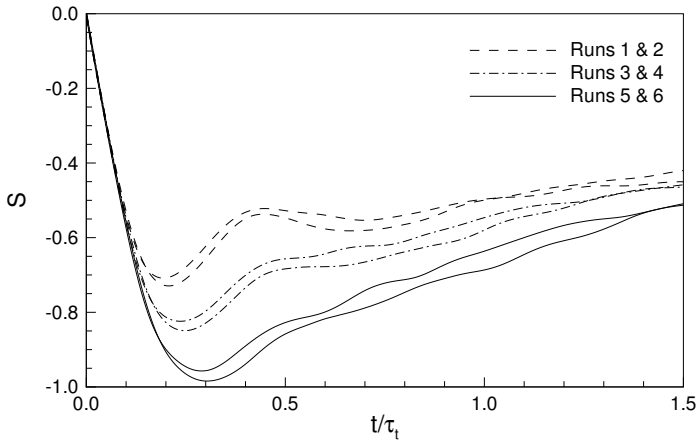

Figure 2. Temporal evolution of the velocity derivative skewness.

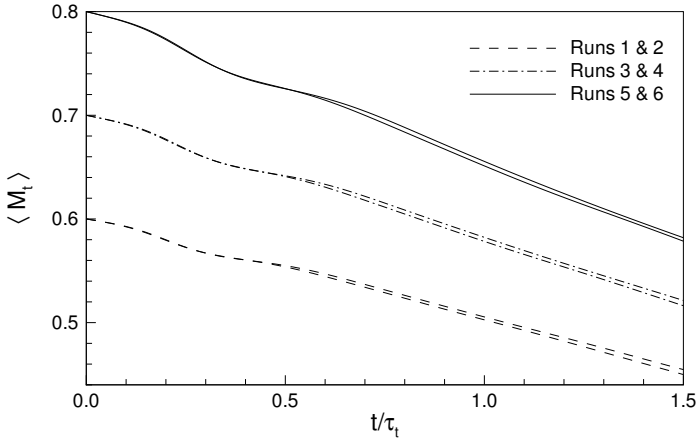

Figure 3. Temporal evolution of the average turbulent mach number M_t.

Our procedure to identify shocklets is based loosely on that of Samtaney et al.,[11] who also investigated isotropic turbulence. We first locate points of inflection in the pressure field by determining the grid points around which the pressure satisfies

$$\nabla^2 p = 0 \tag{13}$$

within some small numeric tolerance. We may further narrow this collection of possible matches after noting that the local velocity vector and pressure gradient should be nearly aligned though exact alignment would hold only for steady normal shocks. Thus the previously flagged points must also have velocities and pressure gradients that satisfy

$$1 - \frac{\vec{u} \cdot \vec{\nabla} p}{|\vec{u}||\vec{\nabla} p|} < \varepsilon \tag{14}$$

in which we have set $\varepsilon = 0.2$, which corresponds to an angle between the two of approximately 35°. The final and most important test is whether the density and pressure ratios across the possible shocklet obey, again within a numeric tolerance, the Rankine-Hugoniot jump conditions,

$$\rho_r - \frac{(\gamma+1)\, p_r + (\gamma-1)}{(\gamma-1)\, p_r + (\gamma+1)} = 0 \tag{15}$$

in which γ is the specific heat capacity ratio. The two density and two pressure values that form these ratios are taken from the endpoints of a straight line, several grid spacings in length, drawn through the grid point of interest in the direction of its local pressure gradient. In order to avoid interpolation, we in practice obtain the density and pressure from the grid points closest to these endpoints rather than the endpoints themselves. Figure 4 provides a schematic of this process.

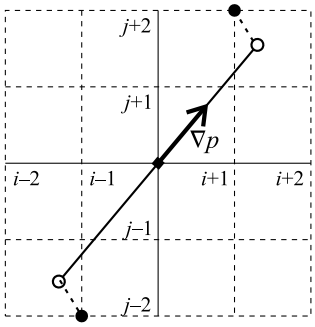

Figure 4. Determining the two points from which to take values of density and pressure when testing the Rankine-Hugoniot jump conditons.

Because some of the rejected shocklet candidates may, in fact, be shocklets, we cannot simply define shock-free regions as all of those grid points that we have determined do not straddle shocklets. Instead we consider a subset of shock-free regions in which the pressure is constant. If at every point within a small radius of a certain grid point the pressure deviates from its global average by no more than a numeric tolerance, we designate that point to be shock-free.

Figure 5 shows representative density and pressure profiles along a streamline through one of the grid points that our search algorithm flagged as a shocklet. The distance along the streamline L, relative to the point of interest, is normalized by the grid spacing Δ, which is the same in all three directions. Symbols demarcate the region between the points closest to those at which the Rankine-Hugoniot jump conditions were tested. The shocklet here is weak and not clearly delineated from the surrounding flow. We have found this situation to be typical, and thus an accurate determination of shocklet strength is rather difficult.

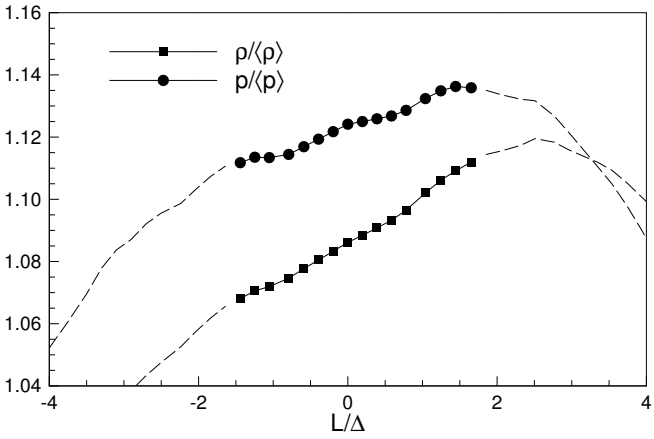

Figure 5. Density and pressure profiles along a streamline through one of the grid points of Run 5 flagged as a shocklet. Flow is from left to right.

VI. Measures of Adaption

In order to analyze the local behavior of the WENO adapton mechanism, we first require quantitative values that convey useful information regarding local stencil adaption. Weirs[1] proposed two such measures: the centrality and nonlinearity indices. Both are combinations of sums involving the final computed stencil weights α_k, which become the weights ω_k of Section III when normalized, relative to the optimal weights C_k.

The centrality index CI is a measure of stencil symmetry:

$$CI = \left[\sum_{k=0}^{r} \frac{k\,(\alpha_k / C_k)}{\sum_{k=0}^{r} (\alpha_k / C_k)} \right] - \frac{r}{2} \tag{16}$$

A value of zero indicates that the final numerical stencil is perfectly symmetric although it may still deviate substantially from the optimal stencil. If CI is negative, upwinding takes place, along with associated dissipation, so dissipation increases with departure from $CI = 0$. Theoretically, positive values would suggest downwinding, but this, as was previously mentioned, is prohibited for reasons of stability. For our particular WENO sheme, the possible range of CI is $[-2 : 0]$.

The nonlinearity index NI is a measure of the degree of departure from the optimal stencil, which, without adaption, would lead to a linear numerical method.

$$NI = \left(\sum_{k=0}^{r} \left[1 - \frac{(r+1)\,(\alpha_k / C_k)}{\sum_{k=0}^{r} (\alpha_k / C_k)} \right]^2 \right)^{\frac{1}{2}} \tag{17}$$

This definition forces the NI to always be non-negative, and only the optimal stencil can provide a value of zero. NI reaches its theoretical maximum when any one candidate stencil is chosen exclusively to form the final numerical stencil. The possible range of NI for our scheme is approximately $[0 : 4.5]$.

These indices have proven useful for characterizing the behavior of the adaption mechanism at least for certain idealized test cases. To demonstrate this, we have calculated the centrality and nonlinearity indices for two simple one-dimensional flow fields. Figure 6a depicts a steady normal shock, in which the shock strength and average density and pressure are typical of those found in the $M_t = 0.8$ simulation of isotropic turbulence. Figure 6b shows a sinusoidal variation of density and pressure with a frequency such that the maximum reach of the WENO scheme is one-half of a wavelength. Again, the average density and pressure are consistent with values from the isotropic turbulence case, and the amplitudes are equal to the respective root-mean-squared values. As expected, the adaption mechanism has engaged strongly at the shock and remains comparatively disengaged for the oscillations that are not shocks.

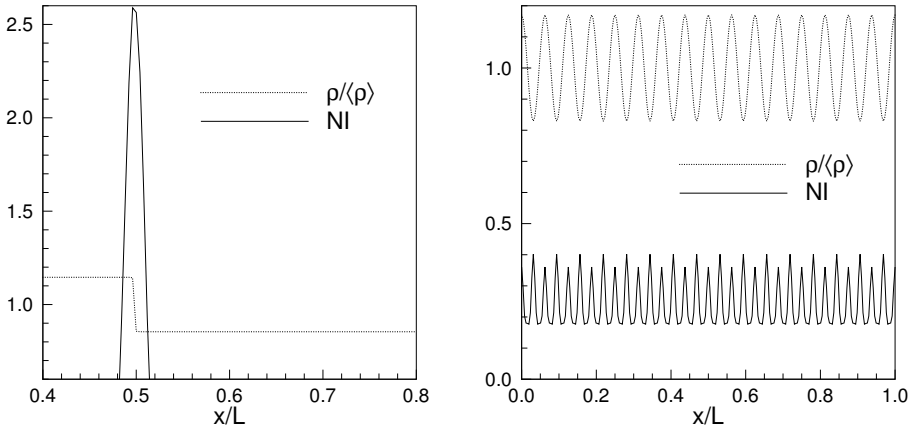

Figure 6. One-dimensional profiles of density and the nonlinearity index for (a) a steady normal shock and (b) sinusoidal oscillations of density and pressure.

VII. Assessment of Adaption Indices

We now investigate these WENO adaption indices within the shock-containing and smooth regions of Run 5, the results of which do not differ significantly from those of the other simulations. Figure 7 plots NI versus a measure of relative shock strength, which is roughly equal to the relative incoming normal mach number of the shocklets. We stress that the absolute magnitudes of these "mach numbers" are not likely to be exactly accurate; however, their relative standing is more firm. We observe that for the chosen conditions the range of shock strengths is exceedingly narrow. Contrary to logical expectations, the degree of WENO stencil adaption as indicated through NI does not appear to depend on the strengths of the shocklets. When NI from within the smooth regions are included for comparison, the data fall more in line with expectations in that the smooth points experience less overall adaption than the shocklets. Nevertheless, the contrast is not nearly as stark as in the ideal case of Fig. 6.

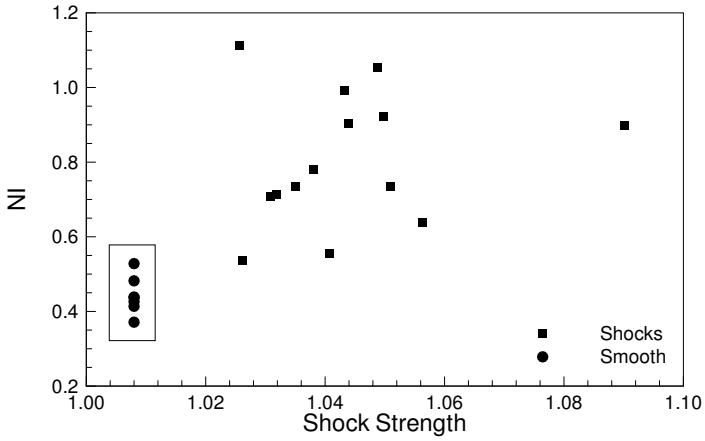

Figure 7. Values of the nonlinearty index near shocklets versus shock strength. Smooth regions are also included for comparison and arbitrarily placed along the independent-variable axis.

Figure 8 displays the range of NI for both shocklets and smooth regions as the grid is coarsened. We use a top-hat filter to transform our 128^3 flow field from Run 5 to resolutions of 64^3 and 32^3 and calculate NI anew for each. Overall NI increases slightly as the grid resolution decreases due to larger perceived variations

from one grid point to the next. The most dramatic difference, however, is the relative values between the shocklets and the smooth regions. As the resolution drops, the NI of the smooth regions moves from the lower portion of the aggregated distribution at 128^3 to the top at 32^3. Figure 9 presents an almost exact mirror of these traits for the CI. Thus WENO stencil adaption is more easily triggered on the coarser grids and leads to greater dissipation in their smooth regions. Though these observations are hardly revolutionary, they do reveal that NI and CI are able to demonstrate such behavior quantitatively.

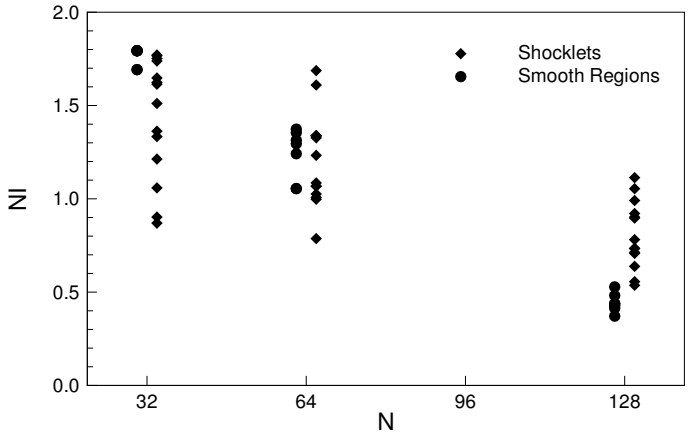

Figure 8. Distribution of values of the nonlinearity index near shocklets and in smooth regions for varying values of the number of grid points per dimension.

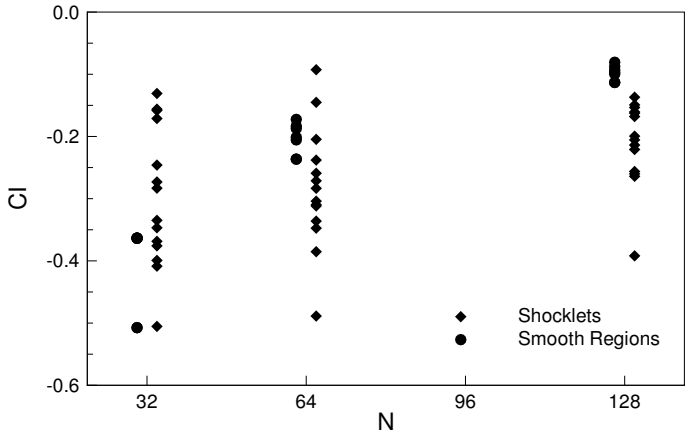

Figure 9. Distribution of values of the centrality index near shocklets and in smooth regions for varying values of the number of grid points per dimension.

VIII. Conclusion

We have performed direct numerical simulations of isotropic turbulence with various initial turbulent mach numbers and find that the range of M_t at the onset of realistic isotropic turbulence does not provide shocklets of sufficiently diverse strengths. Upon comparing the nonlinearity and centrality indices of shock-containing and smooth regions on the 128^3 grid, we observe that the WENO adaption mechanism in general engages more strongly at shocklets than in smooth regions but also that its degree of adaption has no discernible relation to the strengths of the shocklets. Due to the narrow range of strengths considered,

this last is not entirely unexpected. For the chosen conditions, the NI on coarsened grids indicates that the adaption mechanism is more easily triggered in smooth regions as resolution decreases while increasing only slightly in sensitivity in the shock-containing regions. An analysis of the CI under the same conditions confirms that the more pronounced adaption does indeed generate greater dissipation. These preliminary results encourage us to continue to rely upon NI and CI for quantitative local characterization of the WENO stencil adaption mechanism.

Acknowledgments

This work received support from the Air Force Office of Scientific Research grant AF/F49620-02-1-0361 and the National Science Foundation grant CTS-0238390.

References

[1]Weirs, V. G., *A numerical method for the direct simulation of compressible turbulence*, Ph.D. thesis, University of Minnesota, December 1998.

[2]Jiang, G.-S. and Shu, C.-W., "Efficient implementation of weighted ENO schemes," *Journal of Computational Physics*, Vol. 126, No. 1, 1996, pp. 202–28.

[3]Garnier, E., Mossi, M., Sagaut, P., Comte, P., and Deville, M., "On the use of shock-capturing schemes for large-eddy simulations," *Journal of Computational Physics*, Vol. 153, No. 1, 1999, pp. 273–311.

[4]Martín, M. P., "Preliminary DNS database of hypersonic turbulent boundary layers," Paper 2003–3726, American Institute of Aeronautics and Astronautics, 2003.

[5]Martín, M. P., "Hypersonic turbulent boundary layers: Understanding the physics to perform accurate complex simulations," Paper 2004–2337, American Institute of Aeronautics and Astronautics, 2004.

[6]Xu, S. and Martín, M. P., "Assessment of inflow boundary conditions for compressible turbulent boundary layers," *Physics of Fluids*, Vol. 16, No. 7, 2004, pp. 2623–39.

[7]Martín, M. P., "Shock-capturing and the LES of high-speed flows," *Annual Research Briefs*, Center for Turbulence Research, 2000, pp. 193–8.

[8]Blaisdell, G. A. and Ristorcelli, J. R., "Consistent initial conditions for the DNS of compressible turbulence," 49th Annual Meeting of the Division of Fluid Dynamics of the American Physical Society, November 24–26 1996.

[9]Lele, S. K., "Compact finite-difference schemes with spectral-like resolution," *Journal of Computational Physics*, Vol. 103, No. 1, 1992, pp. 16–42.

[10]Lee, S., Lele, S. K., and Moin, P., "Eddy shocklets in decaying compressible turbulence," *Physics of Fluids A*, Vol. 3, No. 4, 1991, pp. 657–64.

[11]Samtaney, R., Pullin, D. I., and Kosović, B., "Direct numerical simulation of decaying compressible turbulence and shocklet statistics," *Physics of Fluids*, Vol. 13, No. 5, 2001, pp. 1415–30.